Computational Particle Mechanics
(will be inserted by the editor)

A FEM-DEM technique for studying the motion of particles in non-Newtonian fluids. Application to the transport of drill cuttings in wellbores

Miguel Angel Celigueta · Kedar M. Deshpande · Salvador Latorre · Eugenio Oñate

Received: date / Accepted: date

Abstract We present a procedure for coupling the finite element method (FEM) and the discrete element method (DEM) for analysis of the motion of particles in non-Newtonian fluids. Particles are assumed to be spherical and immersed in the fluid mesh. A new method for computing the drag force on the particles in a non-Newtonian fluid is presented. A drag force correction for non-spherical particles is proposed. The FEM-DEM coupling procedure is explained for Eulerian and Lagrangian flows and the basic expressions of the discretized solution algorithm are given. The usefulness of the FEM-DEM technique is demonstrated in its application to the transport of drill cuttings in wellbores.

Keywords FEM-DEM procedure · Motion of particles · Drill cuttings · Wellbores

1 INTRODUCTION

The cuttings transport process (hole-cleaning) is one challenging aspect associated with the efficiency of the wellbore drilling operations [1]. This process involves complex interactions between cuttings, drill pipe, wellbore and drilling mud [2]. The investigation of cuttings transport in a wellbore using advanced computational techniques for analysis of particulate non-Newtonian fluids can provide valuable insight for scientific and practical purposes. The focus of this work is to develop a procedure for coupling the finite element method (FEM) and the discrete element method (DEM) for analysis of the motion of particles in non-Newtonian incompressible fluids such as mud. The goal is to understand the cuttings behavior locally in critical sections of the wellbore during their transport by action of the drilling mud. Methods such as that presented here can provide useful information to estimate hole cleaning duration, find zones in danger of clogging or estimate the hole pressure gradient.

Particles within the fluid are modelled with the DEM. The coupling effects between the particles and the fluid are introduced via an immersed technique [3–5]. The fluid motion is modelled either with an Eulerian stabilized FEM formulation using a fixed mesh, or using a Lagrangian formulation using the Particle Finite Element Method (PFEM) [4, 6–16] for which the mesh evolves in time. For both the Eulerian and the Lagrangian formulations we use a mixed finite element formulation with an equal order linear interpolation for the velocities and the pressure variables.

In the Lagrangian PFEM the convective terms vanish in the momentum equations and no numerical stabilization is needed for these equations. Another source of instability, however, remains in the numerical solution of Lagrangian flows such as PFEM, that due to the treatment of the incompressibility constraint which still requires using a stabilized numerical method. In this work we use a PFEM formulation based on a residual-based stabilized expression of the mass balance equation [10–16]. The excellent mass preservation feature of this formulation has been demonstrated previously [7, 16].

M.A. Celigueta, S. Latorre, E. Oñate
Centre Internacional de Mètodes Numèrics en Enginyeria (CIMNE)
Campus Norte UPC, 08034 Barcelona, Spain
Tel.: +34-93-2057016
Fax: +34-93-4016517
E-mail: maceli,latorre,onate@cimne.upc.edu

K.M. Deshpande
Weatherford International Ltd.
E-mail: Kedar.Deshpande@Weatherford.com

The layout of the paper is the following. In the next section we present the basic equations for the conservation of linear momentum and mass for a quasi-incompressible particulate fluid in Eulerian and Lagrangian frameworks. The different force terms acting on the particles are explained. Details of the computation of the drag force for spherical and non spherical particles in non-Newtonian fluids are given. The finite element discretization is presented and the relevant matrices and vectors of the discretized problem are given. The transient solution of the FEM-DEM equations for a particulate flow using a Newton-Raphson type iterative scheme for solving the fluid equations is presented.

The efficiency and accuracy of the FEM-DEM procedure for analysis of particulate flows in non-Newtonian fluids are verified by solving a number of drilling transport problems in wellbores.

2 DESCRIPTION OF THE FEM-DEM ALGORITHM

2.1 Modelling of the particles

Figure 1 shows a fluid domain containing particles of small and moderate sizes relative to the representative volume for a node. Particles are assumed to have a spherical shape in two and three-dimensions (2D/3D) and are modelled as rigid objects that undergo interaction forces due to the physical contact between a particle and its neighbors, as in the standard DEM [17–20].

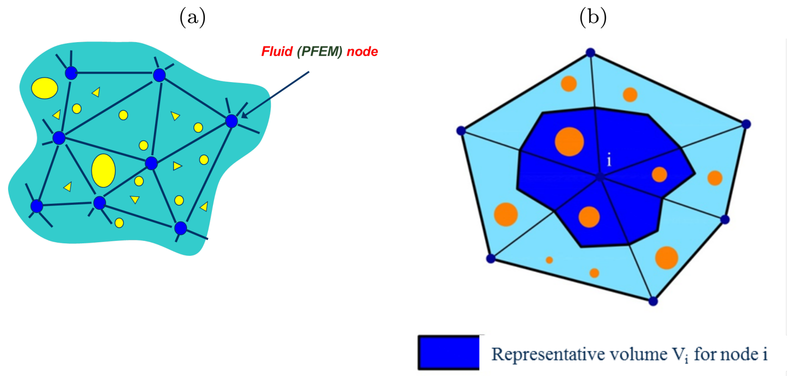

Fig. 1: (a) Particles of different sizes surrounding the nodes in a FEM mesh. (b) Representative volume for a node (in shadowed darker colour)

Fluid-to-particle forces are transferred to the particles via appropriate drag and buoyancy functions. Particle-to-fluid forces have equal magnitude and opposite direction as the fluid-to-particle ones and are transferred to the fluid points as an additional body force vector in the momentum equations (Figure 2). These forces, as well as the mass balance equations account for the percentage of particles in the fluid, similarly as it is done in immersed approaches for particulate flows [4, 5, 17]. The rest of the interaction forces between fluid and particles are neglected (lift forces, virtual mass forces, drag torque, etc.) [21, 22].

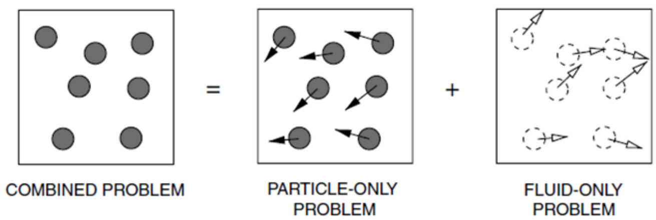

Fig. 2: Immersed approach for treating the motion of physical particles in a fluid [5]

The following sections describe the governing equations for a particulate fluid and the computation of the forces on the particles.

2.2 Basic governing equations for a particulate fluid

2.2.1 Conservation of linear momentum

The equation for linear momentum conservation can be expressed as

$$r_{m_i} = 0 \tag{1a}$$

with

$$r_{m_i} := \rho_f \frac{Dv_i}{Dt} - \frac{\partial \sigma_{ij}}{\partial x_j} - \left(b_i - \frac{1}{n_f} f_i^{pf} \right) \quad , \quad i,j = 1, \cdots, n_s \quad \text{in } V \tag{1b}$$

Summation of terms with repeated indices is assumed in Eq.(1) and in the following, unless otherwise specified.

In Eq.(1) V is the analysis domain, n_s is the number of space dimensions ($n_s = 3$ for 3D problems), ρ_f is the density of the fluid, v_i and b_i are the velocity and body force components along the ith Cartesian axis, respectively, σ_{ij} are the fluid Cauchy stresses, f_i^{pf} are averaged particle-to-fluid interaction forces for which closure relations must be provided and n_f is the fluid volume fraction at a point defined for each node j as

$$n_{f_j} = 1 - \frac{1}{V_j} \sum_{i=1}^{n_j} V_j^i \tag{2}$$

where V_j is the volume of the representative domain associated to a fluid node j, V_j^i is the volume of the ith particle belonging to V_j and n_j is the number of particles contained in V_j. Note that $n_{f_j} = 1$ for a representative fluid domain containing no particles (Figure 1).

The fluid volume fraction n_f in Eq.(1) is a continuous function that is interpolated from the nodal values in the finite element fashion [14, 23, 24].

Remark 1. The time derivative $\frac{Dv_i}{Dt}$ in Eq.(1) is computed in the Eulerian and Lagrangian frameworks as

$$\textit{Eulerian}: \qquad \frac{Dv_i}{Dt} = \frac{\partial v_i}{\partial t} + v_j \frac{\partial v_i}{\partial x_j} \tag{3a}$$

$$\textit{Lagrangian}: \qquad \frac{Dv_i}{Dt} = \frac{\partial v_i}{\partial t} = \frac{{}^{n+1}v_i - {}^{n}v_i}{\Delta t} \tag{3b}$$

with

$${}^{n+1}v_i := v_i({}^{n+1}\mathbf{x}, {}^{n+1}t) \quad , \quad {}^{n}v_i := v_i({}^{n}\mathbf{x}, {}^{n}t) \tag{3c}$$

In Eq.(3c) ${}^{n}v_i({}^{n}\mathbf{x}, {}^{n}t)$ is the velocity of the material point that has the position ${}^{n}\mathbf{x}$ at time $t = {}^{n}t$, where $\mathbf{x} = [x_1, x_2, x_3]^T$ is the coordinates vector of a point in a fixed Cartesian system. Note that the convective term, typical of the Eulerian formulation, does not appear in the definition of the material derivative in Eq.(3b) [24–26].

2.2.2 Constitutive equations

The Cauchy stresses in the fluid, σ_{ij}, are split into the deviatoric (s_{ij}) and pressure (p) components as

$$\sigma_{ij} = s_{ij} + p\delta_{ij} \tag{4}$$

where δ_{ij} is the Kronecker delta. In this work the pressure is assumed to be positive for a tension state.

The relationship between the deviatoric stresses and the strain rates has the standard form for a Newtonian fluid [24, 26],

$$s_{ij} = 2\mu\varepsilon'_{ij} \quad \text{with } \varepsilon'_{ij} = \varepsilon_{ij} - \frac{1}{3}\varepsilon_v \delta_{ij} \quad \text{and} \quad \varepsilon_v = \varepsilon_{ii} \tag{5}$$

In Eq.(5), μ is the viscosity and ε'_{ij} and ε_v are the deviatoric and volumetric strain rates, respectively. The strain rates, ε_{ij}, are related to the velocities by

$$\varepsilon_{ij} = \frac{1}{2} \left(\frac{\partial v_i}{\partial x_j} + \frac{\partial v_j}{\partial x_i} \right) \tag{6}$$

For the non-Newtonian fluids considered in this work the viscosity dependence with the strain rate is defined as

$$\mu(\gamma) = \frac{\tau(\gamma)}{\gamma} \tag{7}$$

where the expression of the shear stress, $\tau(\gamma)$, is obtained experimentally from a viscometer test. For multidimensional flows, γ is defined as the second invariant of the symmetric gradient of the velocity field, i.e.

$$\gamma = \sqrt{\frac{1}{2}\varepsilon_{ij}\varepsilon_{ij}} \tag{8}$$

2.2.3 Mass conservation equation

The mass conservation equation for a particulate flow is written as

$$r_v = 0 \tag{9a}$$

with

$$r_v := \frac{D(n_f \rho_f)}{Dt} + n_f \rho_f \varepsilon_v \tag{9b}$$

Expanding the term and dividing Eq.(9a) by $n_f \rho_f$, the expression of r_v can be redefined as

$$r_v := -\frac{1}{\kappa}\frac{Dp}{Dt} + \frac{1}{n_f}\frac{Dn_f}{Dt} + \varepsilon_v \tag{10}$$

where κ ($\kappa = \rho_f c^2$) is the bulk compressibility parameter, c being the speed of sound and $c^2 = -\frac{\partial p}{\partial \rho}$.

Remark 2. For $n_f = 1$, no particles are contained in the fluid. Consequently, $f_i^{\rho f} = 0$ and the standard momentum and mass conservation equations for a viscous fluid are recovered [24, 26].

Remark 3. Similarly as in Eqs.(2.2.1) the time derivative term in Eqs.(9b) and (10) has different forms in Eulerian and Lagrangian frameworks, i.e.

$$\textit{Eulerian}: \qquad \frac{D(\cdot)}{Dt} = \frac{\partial(\cdot)}{\partial t} + v_j \frac{\partial(\cdot)}{\partial x_j} \tag{11}$$

$$\textit{Lagrangian}: \qquad \frac{D(\cdot)}{Dt} = \frac{\partial(\cdot)}{\partial t} = \frac{{}^{n+1}(\cdot) - {}^{n}(\cdot)}{\Delta t} \tag{12}$$

with ${}^{n}(\cdot)$ having the same meaning as in Eq.(3b).

2.2.4 Boundary conditions

The boundary conditions at the Dirichlet (Γ_v) and Neumann (Γ_t) boundaries with the fluid boundary $\Gamma = \Gamma_v \cup \Gamma_t$ are

$$v_i - v_i^p = 0 \qquad \text{on } \Gamma_v \tag{13a}$$

$$\sigma_{ij} n_j - t_i^p = 0 \qquad \text{on } \Gamma_t \quad i,j = 1, \cdots, n_s \tag{13b}$$

where v_i^p and t_i^p are the prescribed velocities and prescribed tractions at the Γ_v and Γ_t boundaries, respectively and n_j are the components of the unit normal vector to the boundary [24–26].

At a free surface the Neumann boundary conditions (Eq.(13b)) apply. These conditions are enforced at every time step.

2.3 Motion of particles

The motion of particles follows the standard law for Lagrangian particles. For the ith particle

$$m_i\dot{\mathbf{u}}_i = \mathbf{F}_i \quad , \quad J_i\dot{\mathbf{w}}_i = \mathbf{T}_i \tag{14}$$

where $\mathbf{u}_i$ and $\mathbf{w}_i$ are the velocity and the rotation vector of the center of gravity of the particle, m_i and J_i are the mass and rotational inertia of the particle, respectively and $\mathbf{F}_i$ and $\mathbf{T}_i$ are the vectors containing the forces and torques acting at the gravity center of the particle [19, 20].

Eqs.(14) are integrated in time in order to compute the motion of the particles. An explicit Forward Euler scheme has been used with substeppping. The substepping is necessary to avoid instabilities in the DEM solution since the fluid time steps are usually too large for the DEM solver. The information of the fluid which is projected to the particles is interpolated linearly between two steps of the fluid solution to the substep of the DEM solution.

The forces $\mathbf{F}_i$ acting on the ith particle are computed as

$$\mathbf{F}_i = \mathbf{F}_i^w + \mathbf{F}_i^c + \mathbf{F}_i^{fp} \tag{15}$$

$\mathbf{F}_i^w$, $\mathbf{F}_i^c$ and $\mathbf{F}_i^{fp}$ are the forces on the particle due to self-weight, contact interactions between particles and fluid effects. These forces are computed as follows.

2.3.1 Self-weight forces

The self-weight force acting on a particle can be written as

$$\mathbf{F}_i^w = -\rho_i \Omega_i \mathbf{g} \tag{16}$$

where ρ_i and Ω_i are the density and the volume of the ith particle, respectively and $\mathbf{g}$ is the gravity acceleration vector.

2.3.2 Contact forces

The contact forces acting on a particle coming from other particles and walls are summed as follows:

$$\mathbf{F}_i^c = \sum_{j=1}^{n_i} \mathbf{F}_{ij}^c \tag{17}$$

where n_i is the number of contact interfaces for the ith particle.

$$\mathbf{F}_{ij}^c = \mathbf{F}_n^{ij} + \mathbf{F}_s^{ij} = F_n^{ij} n_i + \mathbf{F}_s^{ij} \tag{18}$$

where $\mathbf{F}_n^{ij}$ and $\mathbf{F}_s^{ij}$ are the normal and tangential forces acting at the ith interface connecting particles i and j (Figure 3) or particle i with a wall. These forces are computed in terms of the relative motion of the interacting particles as in the standard DEM [17–20]. Figure 3 summarizes some aspects of the DEM. Figure 3a depicts the particle i with 8 neighbor particles (j, k, l, m, n, p, q and r). Figure 3b shows details of the contact between particles i and j: d_{ij} is the distance between centers, r_c^{ij} is the vector from the center of the particle i to the contact point between i and j, F^{ij} is the force exerted by particle j on particle i at the contact point. Figure 3c shows the scheme of the kinematics of the contact. Both particles have a velocity ($\dot{\mathbf{u}}_i$, $\dot{\mathbf{u}}_j$) and an angular velocity (w_i, w_j). The relative displacement of the particles at the contact point is penalized with elastic constants to avoid interpenetration between particles. Figure 3d shows the decomposition of the relative displacement and the contact force in the normal and tangential directions at the contact point. Figure 3e shows the linear elastic dashpot system used for modeling the mechanical behaviour at a contact point. The elastic penalty constants are K_n (normal direction) and K_s (tangential direction); C_n is a viscous parameter that provides damping to the contact; μ is the Coulomb's friction parameter. It affects the limit at which sliding between particles occurs, which follows the expression $\mathbf{F}_s^{ij} \leq \mu \mathbf{F}_n^{ij}$.

2.3.3 Fluid-to-particle forces

The interaction force between the fluid and a particle is written as $\mathbf{F}_i^{fp} = \mathbf{F}_i^d + \mathbf{F}_i^b$, where $\mathbf{F}_i^b$ and $\mathbf{F}_i^d$ are, respectively, the buoyancy and drag forces on the ith particle. These forces are computed as:

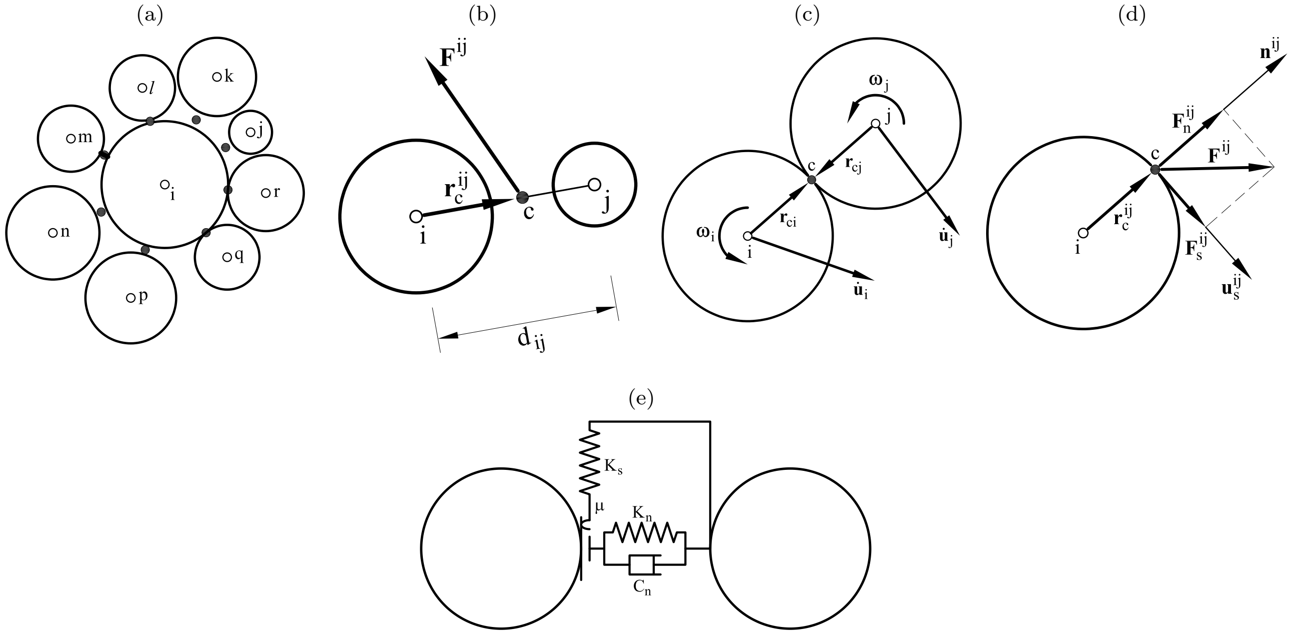

$\mathbf{F}_n^{ij} = K_n \mathbf{u}_n^{ij} + C_n \dot{\mathbf{u}}_n^{ij}$ $\mathbf{u}_n^{ij}, \mathbf{u}_s^{ij}$ relative displacements in the normal and tangential directions to a contact interface

$\mathbf{F}_s^{ij} = K_s \mathbf{u}_s^{ij}$

Fig. 3: (a) Group of eight particles in contact with the ith particles. (b) Contact force vector for two particles interacting with a gap distance. (c) Distance vectors and velocity vector for two particle in contact. (d) Normal and tangential forces and displacement at a contact point. (e) Linear elastic dash pot system modeling the mechanical behaviour at a contact point [20]

2.3.4 Buoyancy forces

The buoyancy force depends on the volume of the particle and the gradient of pressure of the fluid:

$$\mathbf{F}_i^b = -\Omega_i \boldsymbol{\nabla} p \tag{19}$$

Note that $\boldsymbol{\nabla} p$ is not always aligned with gravity, but depends on the fluid dynamics.

2.3.5 Drag forces

The drag force is defined as

$$\mathbf{F}_i^d = -F_i^d \hat{\mathbf{v}}_i^r \tag{20}$$

where

$$\hat{\mathbf{v}}_i^r = \frac{\mathbf{v}_i^r}{|\mathbf{v}_i^r|} \quad \text{with} \quad \mathbf{v}_i^r = \mathbf{u}_i - \mathbf{v}_i \tag{21}$$

is the relative velocity of the particle with respect to the fluid, with $\mathbf{v}_i$ being the velocity vector of the fluid point coinciding with the ith particle.

The computation of the drag force F_i^d is explained in the next section.

2.3.6 Computation of f_i^{pf}

The force term component f_i^{pf} in the right hand side of the momentum equations (Eq.(1)) is computed for each particle (in vector form) as $\mathbf{f}^{pf} = -\mathbf{f}^{fp}$ with vector $\mathbf{f}^{fp}$ computed *at each node* in the fluid mesh from the drag forces $\mathbf{F}_i^d$ as

$$\mathbf{f}_j^{fp} = \frac{1}{V_j} \sum_{i=1}^{n_j} N_j(x_i) \mathbf{F}_i^d \quad , \quad j = 1, N \tag{22}$$

where $N_j(x_i)$ is the value of the shape function of node j at the position of the ith particle.

A continuum distribution of $\mathbf{f}^{fp}$ is obtained by interpolating its nodal values over each element in the FEM fashion.

The forces on the particles due to lift effects have been neglected in the present analysis. These forces can be accounted for as explained in [27].

2.4 Computation of the drag force $\mathbf{F}_i^d$ for non-Newtonian fluids

The drag forces on particles immersed in a Newtonian fluid [28] are well known. However, when dealing with non-Newtonian fluids different approaches for computing these forces can be followed depending on the type of fluid. Non-Newtonian fluids, for example, can be shear thickening, shear thinning or Bingham plastics, and each one of these requires a different drag law. Most drag laws require finding a suitable value for the drag coefficient (C_d) and the Reynold's number.

Drilling fluids for the oil-drilling industry usually exhibit a Herschel-Bulkley behavior [1]. Drag laws for particles moving in drilling fluids based on a shear thickening behavior can be discarded. On the other hand, drag laws developed under the assumptions of a Bingham plastic [29–31] fail to predict accurately the drag force when they are applied to Herschel-Bulkley fluids. In fact, no drag laws for particles in Herschel-Bulkley fluids, or in fluids characterized by a power law rheogram are found in the literature.

Despite the lack of suitable drag laws for particles in Herschel-Bulkley fluids, some accurate estimations of the terminal velocity of the particle (i.e. the steady state velocity reached by a particle falling freely in a liquid) can be found in several papers for different fluids [21, 32]. In particular, Shah [33] proposed an estimation of the terminal velocity in power law fluids characterized by the following value of the (non linear) viscosity

$$\mu(\gamma) = K\gamma^{n-1} \tag{23}$$

where γ was defined in Eq.(8), and K and n are material parameters. Shah's method has proven to give good estimations of the terminal velocity of particles falling in drilling muds in accordance to published experiments [31] (see Figure 4). The terminal velocity will be used later on in this section to generate a drag law.

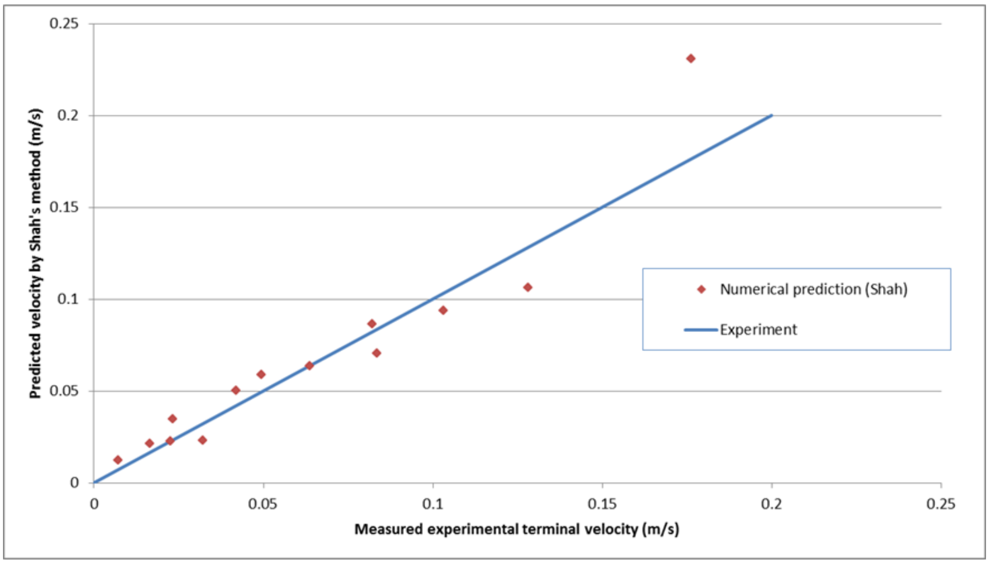

Fig. 4: Relation between the experimental terminal velocity and the values predicted by Shah's method [33]. The straight line indicates the exact correlation between experimental and predicted values [31]

2.4.1 Computation of the terminal velocity of the particles

In the following lines we summarize the steps for estimating the terminal velocity of the particles using Shah's method.

1. Compute

$$A = 6.9148(n^2) - 24.838(n) + 22.642 \quad \text{and} \quad B = -0.5067(n^2) + 1.3234(n) - 0.1744 \tag{24}$$

where n is the power exponent in Eq.(23).

2. Obtain Shah's dimensionless parameter S_i for the ith particle as

$$S_i = (C_d^t)^{\frac{2-n}{2}} Re_t^i \tag{25}$$

where the drag coefficient for the ith particle is defined as

$$C_d^i = \frac{4}{3}\left(\frac{d_p^i g}{(v_t^i)^2}\right)\left(\frac{\rho_p^i - \rho_f}{\rho_f}\right) \tag{26}$$

with

$$Re_t^i = \frac{(d_p^i)^n (v_t^i)^{2-n} \rho_f}{2^{n-1} K} \tag{27}$$

being the Reynolds number at the terminal velocity for power law fluids (other authors such as Walker *et al.* [34, 35] give other definition for Re). In Eq.(26) g is the gravity acceleration, d_i is the particle diameter and K is the parameter in Eq.(23).

Substituting Eqs.(26) and (27) into (25) Shah's dimensionless parameter can be computed as

$$S_i = \frac{1}{2^{n-1}K}\sqrt{\left(\frac{4}{3}\right)^{2-n} (d_p^i)^{n+2} \rho_f^n (\rho_p^i - \rho_f)^{2-n} g^{2-n}} \tag{28}$$

Note that Eq.(28) does not depend on v_t^i.

3. Obtain the Reynolds number for the ith particle from

$$Re_t^i = \left(\frac{S_i}{A}\right)^{\frac{1}{B}} \tag{29}$$

4. The terminal velocity for the ith particle v_t^i is computed from Eq.(27) as

$$v_t^i = \left[\frac{2^{n-1} K Re_t^i}{(d_p^i)^n \rho_f}\right]^{\frac{1}{(2-n)}} \tag{30}$$

2.4.2 Computation of the drag force

In this work a linear drag force law is proposed for cuttings moving in drilling muds of the type

$$F_i^d(v_i^r) = a_i s_i + \frac{W_i - F_i^b - a_i s_i}{v_t^i} v_i^r \tag{31}$$

where a_i is a parameter that is a function of the gel strength of the fluid and its dynamics [1], s_i is the surface area of the particle, $W_i = |\mathbf{F}_i^w|$ is the weight of the particle, F_i^b the modulus of the buoyancy force vector ($F_i^b = |\mathbf{F}_i^b|$), v_i^r is the relative velocity of the particle with respect to to the fluid ($v_i^r = |\mathbf{v}_i^r|$, see Eq.(23)) and v_t^i is the relative terminal velocity obtained by Shah's method via Eq.(30). Note that for $v_i^r = v_t^i$ the equilibrium of forces for the terminal slip velocity is recovered (i.e. $F_i^d = W_i - F_i^b$). On the other hand, for $v_i^r = 0$ the initial force (gel strength) is recovered.

The gel strength is the maximum stress the fluid can withstand before showing some measurable shear rate. For those cases when $v_i^r = 0$ the drag law presents a singularity and its derivative is infinite. This means that the force can be any value between 0 and $a_i\, s_i$. To solve this problem, the drag force law must be regularized. In this work we have modified the drag force as

$$\bar{F}_i^d(v_i^r) = \frac{F_i^d(\hat{v}_i^r)}{\hat{v}_i^r} v_i^r \quad \text{for } v_i^r \in [0, \hat{v}_i^r] \tag{32}$$

where $\hat{v}_i^r$ is a very small value.

Note that a_i is equal to the gel strength for every part of the fluid where the equivalent shear rate is zero. However, in those parts of the fluid where the shear rate is not zero, the apparent viscosity perceived by the particle decreases. In this situation, the gel strength has already been overcome and a_i must be set to zero.

2.4.3 Accounting for the effect of the non sphericity of the particles

The sphericity coefficient (Ψ) is defined as the ratio between the skin surface of the non-spherical particle and the skin surface of a sphere with the same volume. For the same relative velocity of the particle with respect to the fluid, the drag force grows as the sphericity decreases. Although some authors use the sphericity coefficient within a range between 0.125 and 1.0 [1] it must be pointed out that very low values of Ψ correspond actually to shapes that are far from spherical (plates, flat discs, thin sticks, ...). In those cases, the correction that Ψ brings to the equations that assume spherical shape can be very wrong. The authors do not recommended using Ψ below 0.65.

Different authors have established the dependency of the drag coefficient with the Reynolds number and the sphericity parameter for Newtonian fluids. For instance, Chien [32] proposed

$$C_d = \frac{30}{Re} + 67.289e^{(-5.03\Psi)} \tag{33}$$

while Haider and Levenspiel [36] propose:

$$C_d = \frac{24}{Re}\left[1 + \exp(2.3288 - 6.4581\Psi + 2.4486\Psi^2)Re^{(0.0964+0.5565\Psi)}\right] + \frac{73.69Re \cdot \exp(-5.0748\Psi)}{Re + 5.378\exp(6.2122\Psi)} \tag{34}$$

Both expressions and others mentioned in [31] can be used to obtain the drag coefficient for spherical particles simply making $\Psi = 1$.

In order to include the effect of the non sphericity of the particles in Shah's method, the dimensionless parameter S_i (Eq.(25)) has to be modified. This can be done by substituting the drag coefficient by an equivalent one which accounts for the sphericity effect. For that purpose, the following parameter is used:

$$\varphi^i = \frac{C^i_{d,non-sphere}}{C^i_{d,sphere}} \tag{35}$$

where φ^i is the ratio of drag coefficients for a particle in Newtonian fluids computed via Eqs.(33) or (34).

Taking into account that C_d in Eq.(25) corresponds to an spherical particle, Shah's dimensionless parameter is re-written using Eq.(35) as :

$$S_i = \left(\frac{C^i_{d,non-sphere}}{\varphi^i}\right)^{\frac{2-n}{2}} Re^i_t \tag{36}$$

Eq.(26) holds for both spherical and non-spherical particles. For non-spherical particles d^i_p is the diameter of the sphere with the same volume. Note that A and B were obtained for spherical particles in Eq.(24). This is why C^i_d must be divided by φ^i in order to compute the correct (equivalent) expression of C_d for a spherical particle.

The two-step procedure to compute the drag force for non-spherical particles is as follows:

1. Compute the terminal velocity for the particles using the standard Shah's method (Eq.(30)) where d_i is the equivalent diameter for the non-spherical particle.
2. Compute the drag coefficient for spherical ($\varphi = 1$) and non-spherical ($\varphi \neq 1$) particles via Eqs.(33) or (34) using the Reynolds number of Eq.(29).
3. Compute the value of φ^i.
4. Update S_i as $S^2_i = S^1_i(\varphi^i)^{\frac{2}{2-n}}$, where S^1_i is the value of Shah's parameter computed using Eq.(28).
5. With the updated Shah's parameter, perform the rest of operations in Eqs.(29)–(31).
   The terminal velocity and the drag force obtained after this second step includes the effect of the non sphericity of the particle.

2.5 Discretization of the fluid equations

The modelling of incompressible fluids with a mixed finite element method using an equal order interpolation for the velocities and the pressure requires introducing a stabilized formulation for the mass balance equation.

In our work we use a stabilized form of the momentum mass balance equations obtained via the Finite Calculus (FIC) technique [12, 16, 19, 37] written as

$$r_{m_i} - \underline{\frac{h_{ij}}{2}\frac{\partial r_{m_i}}{\partial x_j}} = 0 \quad \text{in } V \tag{37a}$$

$$r_v - \tau_s \frac{\partial \bar{r}_{m_i}}{\partial x_i} = 0 \quad \text{in } V \tag{37b}$$

where

$$\bar{r}_{m_i} = \frac{\partial \sigma_{ij}}{\partial x_j} + b_i + \frac{1}{n_f} f_i^{pf} \tag{38}$$

is a static momentum term and τ_s is a stabilization parameter computed as

$$\tau_s = \left(\frac{8\mu}{h^2} + \frac{2\rho_f}{\delta} \right)^{-1} \tag{39}$$

In Eqs.(37b) and (39) h_{ij} and h are characteristic length distances that are expressed in terms of the finite element dimensions and δ is a time parameter [12, 16, 19, 37].

The derivation of Eq.(37) for an homogeneous Lagrangian quasi-incompressible fluid is presented in [16].

The stabilization parameter τ is computed in practice for each element e using $h = l^e$ and $\delta = \Delta t$ as

$$\tau_s = \left(\frac{8\mu}{(l^e)^2} + \frac{2\rho}{\Delta t} \right)^{-1} \tag{40}$$

where Δt is the time step used for the transient solution and l^e is a characteristic element length computed as $l^e = 2(V^e)^{1/n_s}$ where V^e is the element area (for 3-noded triangles) or volume (for 4-noded tetrahedra). For fluids with heterogeneous material properties the values of μ and ρ in Eq.(40) are computed at the element center.

2.5.1 Variational equations for the fluid

The variational form of the momentum and mass balance equations is obtained via the standard weighted residual approach [16, 23–26]. The resulting integral expressions after integration by parts and some algebra are:

2.5.2 Momentum equations

The momentum equations can be written as

$$\int_V w_i \rho \frac{Dv_i}{Dt} dV + \int_V \left[\delta\varepsilon_{ij} 2\mu\varepsilon'_{ij} + \delta\varepsilon_v p\right] dV - \int_V w_i \left(b_i + \frac{1}{n_f} f_i^{pf} \right) dV - \int_{\Gamma_t} w_i t_i^p d\Gamma + \underline{\int_V \frac{\partial W_i}{\partial x_j} \frac{h_{ij}}{2} r_{m_i} dV} = 0 \tag{41}$$

2.5.3 Mass balance equation

The mass balance equation can be written as

$$\begin{aligned} \int_V \frac{q}{\kappa} \frac{Dp}{Dt} dV - \int_V q \left(\frac{1}{n_f} \frac{Dn_f}{Dt} + \varepsilon_v \right) dV + \int_V \tau_s \frac{\partial q}{\partial x_i} \left(\frac{\partial}{\partial x_i} (2\mu\varepsilon_{ij}) + \frac{\partial p}{\partial x_i} + b_i \right) dV \\ - \int_{\Gamma_t} q\tau \left[\rho \frac{Dv_n}{Dt} - \frac{2}{h_n} (2\mu \frac{\partial v_n}{\partial n} + p - t_n) \right] d\Gamma = 0 \end{aligned} \tag{42}$$

where h_n is a characteristic length size of an element adjacent to the boundary. For instance in our work h_n is taken as the square root of twice the element area for a triangle.

The derivation of Eqs.(41) and (42) for homogeneous Lagrangian fluids can be found in [16]. Their applications in the context of particulate Newtonian Lagrangian fluids is presented in [4].

Remark 4. For Lagrangian fluids the underlined stabilized terms in Eqs.(37) and (41) are zero.

2.5.4 FEM discretization

We discretize the analysis domain containing N_p particles into finite elements with n_e nodes in the standard manner leading to a mesh with a total number of N_e elements and N nodes. In our work we will choose simple 3-noded linear triangles ($n_e = 3$) for 2D problems and 4-noded tetrahedra ($n_e = 4$) for 3D problems with local linear shape functions N_i^e defined for each node i of element e [14, 23, 25]. The velocity components, the weighting functions and the pressure are interpolated over the mesh in terms of their nodal values in the same manner using the global linear shape functions, N_j, spanning over the elements sharing node j ($j = 1, N$) [14, 23, 25].

The finite element interpolation over the fluid domain can be written in matrix form as

$$\mathbf{v} = \mathbf{N}_v \bar{\mathbf{v}}\ ,\ \mathbf{w} = \mathbf{N}_v \bar{\mathbf{w}}\ ,\ p = \mathbf{N}_p \bar{\mathbf{p}}\ ,\ q = \mathbf{N}_p \bar{\mathbf{q}} \tag{43}$$

where

$$\bar{\mathbf{v}} = \begin{Bmatrix} \bar{\mathbf{v}}^1 \\ \bar{\mathbf{v}}^2 \\ \vdots \\ \bar{\mathbf{v}}^N \end{Bmatrix} \quad \text{with } \bar{\mathbf{v}}^i = \begin{Bmatrix} \bar{v}_1^i \\ \bar{v}_2^i \\ \bar{v}_3^i \end{Bmatrix}\ ,\ \bar{\mathbf{w}} = \begin{Bmatrix} \bar{\mathbf{w}}^1 \\ \bar{\mathbf{w}}^2 \\ \vdots \\ \bar{\mathbf{w}}^N \end{Bmatrix} \quad \text{with } \bar{\mathbf{w}}^i = \begin{Bmatrix} \bar{w}_1^i \\ \bar{w}_2^i \\ \bar{w}_3^i \end{Bmatrix}\ ,\ \bar{\mathbf{p}} = \begin{Bmatrix} \bar{p}^1 \\ \bar{p}^2 \\ \vdots \\ \bar{p}^N \end{Bmatrix} \quad \text{and } \bar{\mathbf{q}} = \begin{Bmatrix} \bar{q}^1 \\ \bar{q}^2 \\ \vdots \\ \bar{q}^N \end{Bmatrix} \tag{44}$$

$$\mathbf{N}_v = [\mathbf{N}_1, \mathbf{N}_2, \cdots, \mathbf{N}_N]^T\ ,\ \mathbf{N}_p = [N_1, N_2, \cdots, N_N]$$

with $\mathbf{N}_j = N_j \mathbf{I}_{n_s}$, where $\mathbf{I}_{n_s}$ is the $n_s \times n_s$ unit matrix.

In Eq.(44), vectors $\bar{\mathbf{v}}$, $\bar{\mathbf{w}}, \bar{\mathbf{q}}$ and $\bar{\mathbf{p}}$ contain the nodal velocities, the nodal weighting functions and the nodal pressures for the whole mesh, respectively and the upper index denotes the nodal value for each vector or scalar magnitude.

Substituting the approximation (43) into the variational forms (41) and (42) gives the system of algebraic equations for the particulate fluid in matrix form as

$$\mathbf{M}_0 \dot{\bar{\mathbf{v}}} + (\mathbf{K} + \mathbf{A} + \mathbf{S})\bar{\mathbf{v}} + \mathbf{Q}\bar{\mathbf{p}} - \mathbf{f}_v = \mathbf{0} \tag{45a}$$

$$\mathbf{M}_1 \dot{\bar{\mathbf{p}}} - \mathbf{Q}^T \bar{\mathbf{v}} + (\mathbf{L} + \mathbf{M}_b)\bar{\mathbf{p}} - \mathbf{f}_p = \mathbf{0} \tag{45b}$$

where

$$\mathbf{M}_{0_{ij}}^e = \int_{\Omega^e} \rho N_i^e N_j \mathbf{I}_3 d\Omega \quad , \quad \mathbf{K}_{ij}^e = \int_{\Omega^e} \mathbf{B}_i^{eT} \mathbf{D} \mathbf{B}_j^e d\Omega \quad \text{and} \quad \mathbf{D} = \mu \begin{bmatrix} 2 & 0 & 0 \\ 0 & 2 & 0 \\ 0 & 0 & 1 \end{bmatrix} \quad , \quad \mathbf{B}_i = \begin{bmatrix} \frac{\partial N_i}{\partial x_1} & 0 \\ 0 & \frac{\partial N_i}{\partial x_2} \\ \frac{\partial N_i}{\partial x_2} & \frac{\partial N_i}{\partial x_1} \end{bmatrix} \quad \text{(for 2D)}$$

$$\mathbf{A}_{ij}^e = \left[\int_{\Omega^e} N_i (\rho \mathbf{u}^T \boldsymbol{\nabla}^T N_j) d\Omega \right] \mathbf{I}_3 \quad , \quad \mathbf{S}_{ij}^e = \left(\int_{\Omega^e} \boldsymbol{\nabla}^T N_i \hat{\mathbf{D}} \boldsymbol{\nabla} N_j d\Omega \right) \mathbf{I}_3$$

$$\mathbf{Q}_{ij}^e = \int_{\Omega^e} \mathbf{B}_i^{eT} \mathbf{m} N_j^e d\Omega \quad , \quad M_{1_{ij}}^e = \int_{\Omega^e} \frac{1}{\kappa} N_i^e N_j^e d\Omega \quad , \quad M_{b_{ij}}^e = \int_{\Gamma_t} \frac{2\tau_s}{h_n} N_i^e N_j^e d\Gamma$$

$$\mathbf{L}_{ij}^e = \int_{\Omega^e} \tau_s (\boldsymbol{\nabla}^T N_i^e) \boldsymbol{\nabla} N_j^e d\Omega \quad , \quad \mathbf{f}_{v_i}^e = \int_{\Omega^e} \mathbf{N}_i^e \mathbf{b} d\Omega + \int_{\Gamma_t} \mathbf{N}_i^e \mathbf{t} d\Gamma$$

$$f_{p_i}^e = \int_{\Gamma_t} \tau_s N_i^e \left[\rho \frac{D v_n}{Dt} - \frac{2}{h_n}(2\mu\varepsilon_n - t_n) \right] d\Gamma - \int_{\Omega^e} \tau_s \boldsymbol{\nabla}^T N_i^e \mathbf{b} d\Omega \qquad \text{with} \quad i, j = 1, n_s$$

In the expressions of $\mathbf{A}_{ij}^e$ and $\mathbf{S}_{ij}^e$, $\mathbf{I}_3$ is the 3×3 unit matrix and $\hat{\mathbf{D}} = \frac{\rho}{2} \mathbf{h} \mathbf{u}^T$, with $\mathbf{h}$ being a characteristic length parameter. A typical definition of $\mathbf{h}$ is

$$\mathbf{h} = h_s \frac{\mathbf{u}}{u} + h_c \frac{\boldsymbol{\nabla} u}{|\boldsymbol{\nabla} u|} \tag{46}$$

where $u = |\mathbf{u}|$ and h_s and h_c are "streamline" and "cross wind" characteristic lengths given by $h_s = \max(l_j^T \mathbf{u})/u$ and $h_c = \max(l_j^T \boldsymbol{\nabla} \mathbf{u})/|\boldsymbol{\nabla} u|$, where j ranges from one to the number of element sides and l_j is the vector defining the jth element side [12].

In Eq.(45a), $\mathbf{K}$, $\mathbf{A}$ and $\mathbf{S}$ are matrices emanating from the viscosity, the advection terms and the stabilization terms in the momentum equations. Matrices $\mathbf{A}$ and $\mathbf{S}$ are zero for Lagrangian flows. The derivation of the matrices and vectors in Eqs.(45) for Eulerian and Lagrangian flows can be found in [12, 16].

2.5.5 Incremental solution of the discretized equations

Eqs.(45) are solved in time with an implicit Newton-Raphson type iterative scheme [23–26]. The basic steps within a time interval $[n, n+1]$ are:

- Generate a new mesh using the position of the fluid nodes at t_n. This step is required for a Lagrangian formulation (such as PFEM) only.
- Initialize variables: $({}^{n+1}\mathbf{x}^1, {}^{n+1}\bar{\mathbf{v}}^1, {}^{n+1}\bar{\mathbf{p}}^1, {}^{n+1}n_f^i, {}^{n+1}\bar{\mathbf{r}}_m^1) \equiv \{{}^n\mathbf{x}, {}^n\bar{\mathbf{v}}, {}^n\bar{\mathbf{p}}, {}^n n_f, {}^n\bar{\mathbf{r}}_m\}$.
- Iteration loop: $k = 1, \cdots, NITER$.
  For each iteration.

Step 1. Compute the nodal velocity increments $\Delta\bar{\mathbf{v}}$

From Eq.(45a), we deduce

$$ {}^{n+1}\mathbf{H}_v^i \Delta\bar{\mathbf{v}} = -{}^{n+1}\bar{\mathbf{r}}_m^k \rightarrow \Delta\bar{\mathbf{v}} \tag{47a}$$

with the momentum residual $\bar{\mathbf{r}}_m$ and the iteration matrix $\mathbf{H}_v$ given by

$$\bar{\mathbf{r}}_m = \mathbf{M}_0\dot{\bar{\mathbf{v}}} + (\mathbf{K}+\mathbf{A}+\mathbf{S})\bar{\mathbf{v}} + \mathbf{Q}\bar{\mathbf{p}} - \mathbf{f}_v \quad , \quad \mathbf{H}_v = \frac{1}{\Delta t}\mathbf{M}_0 + \mathbf{K} + \mathbf{A} + \mathbf{S} + \mathbf{K}_v \tag{47b}$$

where $\mathbf{K}_v^e$ is

$$\mathbf{K}_v^e = \int_{{}^nV^e} \mathbf{B}^T \mathbf{m}\theta\Delta t\kappa\mathbf{m}^T\mathbf{B}dV \tag{47c}$$

The tangent "bulk" stiffness matrix, $\mathbf{K}_v$, accounts for the changes of the pressure due to the velocity. Matrix $\mathbf{K}_v$ in $\mathbf{H}_v$ is important for the fast convergence, mass preservation and overall accuracy of the iterative solution [7, 16].

The parameter θ in $\mathbf{K}_v$ $(0 < \theta \leq 1)$ has the role of preventing the ill-conditioning of the iteration matrix $\mathbf{H}_v$ for quasi-incompressible fluids characterized by very large values of the bulk parameter κ. An adequate selection of θ improves the overall accuracy of the numerical solution and preserves the mass for large time steps [7, 16].

Step 2. Update the velocities

$$\text{Fluid nodes:} \quad {}^{n+1}\bar{\mathbf{v}}^{k+1} = {}^{n+1}\bar{\mathbf{v}}^k + \Delta\bar{\mathbf{v}} \tag{48a}$$

$$\text{Rigid particles:} \quad \begin{cases} {}^{n+1/2}\dot{\mathbf{u}}_j = {}^{n-1/2}\dot{\mathbf{u}}_j + {}^n\ddot{\mathbf{u}}_j^{k+1}\Delta t \\ \dot{\mathbf{u}}_j = \frac{1}{m_j}{}^n\mathbf{F}_j^{k+1} \quad , \quad j = 1, N_p \end{cases} \tag{48b}$$

Step 3. Compute the nodal pressures ${}^{n+1}\bar{\mathbf{p}}^{k+1}$

From Eq.(45b) we obtain

$${}^{n+1}\mathbf{H}_p^i\,{}^{n+1}\bar{\mathbf{p}}^{k+1} = \frac{1}{\Delta t}\mathbf{M}_1\,{}^{n+1}\bar{\mathbf{p}}^i + \mathbf{Q}^T\,{}^{n+1}\bar{\mathbf{v}}^{k+1} + {}^{n+1}\bar{\mathbf{f}}_p^i \rightarrow {}^{n+1}\bar{\mathbf{p}}^{k+1} \tag{49a}$$

with

$$\mathbf{H}_p = \frac{1}{\Delta t}\mathbf{M}_1 + \mathbf{L} + \mathbf{M}_b \tag{49b}$$

Step 4. Update the coordinates of the particles

$$\text{Rigid particles:} \quad \begin{cases} {}^{n+1}\mathbf{u}_i^{k+1} = {}^n\mathbf{u}_i^{k+1} + {}^{n+1/2}\dot{\mathbf{u}}_i^{k+1}\Delta t \\ {}^{n+1}\mathbf{x}_i^{k+1} = {}^n\mathbf{x}_i + {}^{n+1}\mathbf{u}_i^{k+1} \quad , \quad i = 1, N_p \end{cases} \tag{50a}$$

Step 5. Update the coordinate of the fluid nodes (for Lagrangian flows only)

$$\text{Fluid nodes:} \quad {}^{n+1}\mathbf{x}_i^{k+1} = {}^{n+1}\mathbf{x}_i^k + \frac{1}{2}({}^{n+1}\bar{\mathbf{v}}_i^{k+1} + {}^n\bar{\mathbf{v}}_i)\Delta t \quad , \quad i = 1, N \tag{50b}$$

Step 6. Compute the fluid volume fraction for each node ${}^{n+1}n_{f_i}^{k+1}$ *via Eq.(2)*

Step 7. Compute forces and torques on particles: ${}^{n+1}\mathbf{F}_i^{k+1}, {}^{n+1}\mathbf{T}_i^{k+1}$, $i = 1, N_p$

Step 8. Compute particle-to-fluid forces: $({}^{n+1}\mathbf{f}_i^{pf})^{k+1} = -({}^{n+1}\mathbf{f}_i^{fp})^{k+1}$, $i = 1, N$ with $\mathbf{f}_i^{fp}$ computed by Eq.(18)

Step 9. Check convergence

Verify the following conditions:

$$\begin{aligned} \|{}^{n+1}\bar{\mathbf{v}}^{k+1} - {}^{n+1}\bar{\mathbf{v}}^k\| &\le e_v\|{}^n\bar{\mathbf{v}}\| \\ \|{}^{n+1}\bar{\mathbf{p}}^{k+1} - {}^{n+1}\bar{\mathbf{p}}^k\| &\le e_p\|{}^n\bar{\mathbf{p}}\| \end{aligned} \tag{51}$$

where e_v and e_p are prescribed error norms for the nodal velocities and the nodal pressures, respectively. In the examples solved in this work we have set $e_v = e_p = 10^{-3}$.

If both conditions (51) are satisfied, then make $n \leftarrow n + 1$ and proceed to the next time step.

Otherwise, make the iteration counter $k \leftarrow k + 1$ and repeat Steps 1–8.

Remark 5. In Eqs.(47)–(51), ${}^{n+1}(\cdot)$ denote values at time $n+1$. For the Lagrangian formulation using the PFEM the derivatives and integrals in the iteration matrices, $\mathbf{H}_v$ and $\mathbf{H}_p$ and the residual vector $\bar{\mathbf{r}}_m$, are computed on the *discretized geometry at time n* (i.e. $V^e = {}^nV^e$) while the nodal force vectors, $\mathbf{f}_v$ and $\mathbf{f}_p$, are computed on the current configuration at time $n + 1$ [16].

Remark 6. The time step within a time interval $[n, n + 1]$ has been chosen as $\Delta t = \min\left(\frac{{}^nl^e_{\min}}{|{}^n\mathbf{v}|_{\max}}, \Delta t_b\right)$, where ${}^nl^e_{\min}$ is the minimum characteristic distance of all elements in the mesh, with l^e computed as explained in Eq.(40), $|{}^n\mathbf{v}|_{\max}$ is the maximum value of the modulus of the velocity of all nodes in the mesh and Δt_b is the critical time step of all nodes adjacent to a solid boundary [16].

Remark 7. The Eulerian and Lagrangian versions of the formulation have been implemented in the open-source Kratos software platform [38]. The generation of the analysis data and the visualization of the results have been carried out using the GiD pre/postprocessing system [39].

3 EXAMPLES

3.1 Motion of cuttings in a vertical annulus for different fluids

The first problem concerned the study of the transport of cuttings in drilling muds in a vertical wellbore with a centered non-rotating drill string. Numerical results for this problem were obtained with the Lagrangian formulation presented in this work and the PFEM. The average velocity of the particles at a section of the annulus was measured and compared to the average fluid velocity. Non-spherical particles were considered. The drag force was computed as explained in Section 5.1 using the sphericity correction of Eq.(34) [36]. Results are plotted in Figure 5, where experimental data [2] is also shown for comparison. Table 1 shows the rheological properties of the fluids used for defining the viscosity function (Eq.(23)).

	n	K (Pa s^n)	ρ (kg/m^3)
Thick mud	0.33958	3.15275	1030
Intermediate mud	0.37826	1.7637	1030
Water	1	10^{-3}	1030

Table 1: Rheological properties of the fluids used in Figure 5

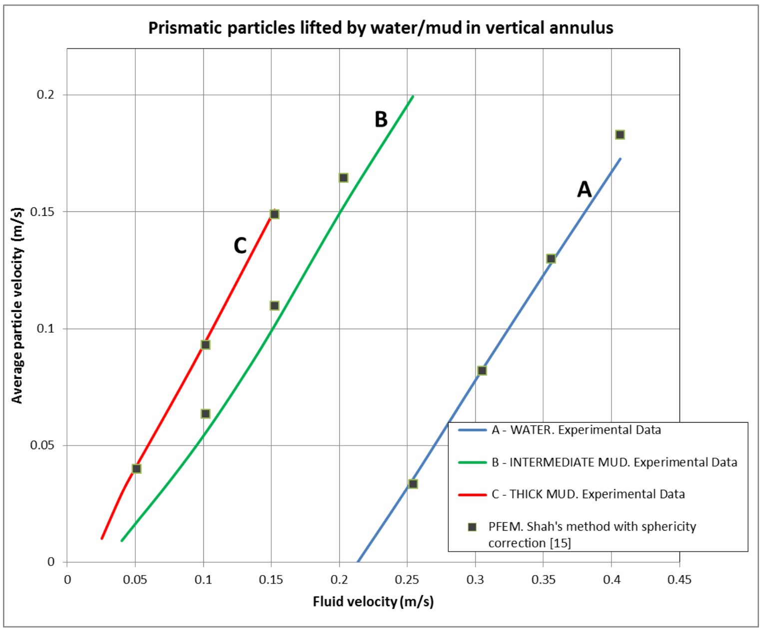

Fig. 5: Average velocity of cuttings velocity vs. fluid velocity for different fluids in a vertical annulus. Lines: Experimental data [2]. Squares: PFEM results

Figure 6 shows results of the motion of the cuttings in a centered drill string, rotating at 10 rpm, which causes the cuttings to move upwards faster. The fluid is an intermediate mud with the following rheogram characteristics $n = 0,37826$ and $K = 1,7637$ Pa s^n (Eq.(23)). Results were obtained using PFEM. The boundary conditions used were the imposed velocity at the inlet, non-slip condition on all was ($\bar{v} = 0$) and free surface at the outlet ($\sigma_{ij} n_j = 0$). The free surface is kept at the same location by removing the nodes crossing the outlet.

The particles have the following characteristics: diameter (4.96 mm), sphericity (0.76766), density (2000 $^{\mathrm{kg}}/_{\mathrm{m}^3}$). These characteristics correspond to particles with the shape of a brick with dimensions $1/8 \times 1/4 \times 1/8$ in, which have been treated as spheres. It must be clarified that the experiments carried out by Sifferman *et al.* [2] were done with fluids with a density of 8.6 $^{\mathrm{le}}/_{\mathrm{gal}}$ (1030 $^{\mathrm{kg}}/_{\mathrm{m}^3}$) and simulated denser fluids with lighter particles.

The DEM contact properties were chosen to just prevent particles from penetrating each other. For this purpose we have used $K_n = 3 \cdot 10^5$ N/m, $K_s = 6,5 \cdot 10^4$ N/m, a Coulomb friction coefficient of $\mu = 0.3$ and the critical damping parameter.

The method to obtain the drag force for non-Newtonian fluids is the one explained in Section 2.4. The example in this section is a vertical wellbore where the slip velocity of the cuttings is close to the terminal velocity, so it is an example well suited for the method. However, the velocity profile in the annulus must be computed accurately and the distribution of the particles, affected by its horizontal velocity, must also be accurate to match the experimental results. Note that the concentration of particles in the section of the annulus is not imposed, but every single particle is injected in a random position of the inlet, and only after some time of ascending motion they reach a steady position in the section. Measurements of the average velocity of the particles were taken close to the outlet.

3.2 Transport of cuttings in inclined and horizontal drilling annulus

The Eulerian and Lagrangian formulations have been applied to the study of the transport of cuttings in inclined and horizontal wellbores that can lead to the formation of particle beds (Figures 7 and 8). The high concentration of particles does not affect the stability of the fluid solver until the size of the cuttings equals the fluid mesh size. The fluid used is the same intermediate mud as in Section 7.1. Results in Figure 7 were obtained using PFEM, while those in Figure 8 were obtained using an Eulerian approach implemented in Kratos [12, 38].

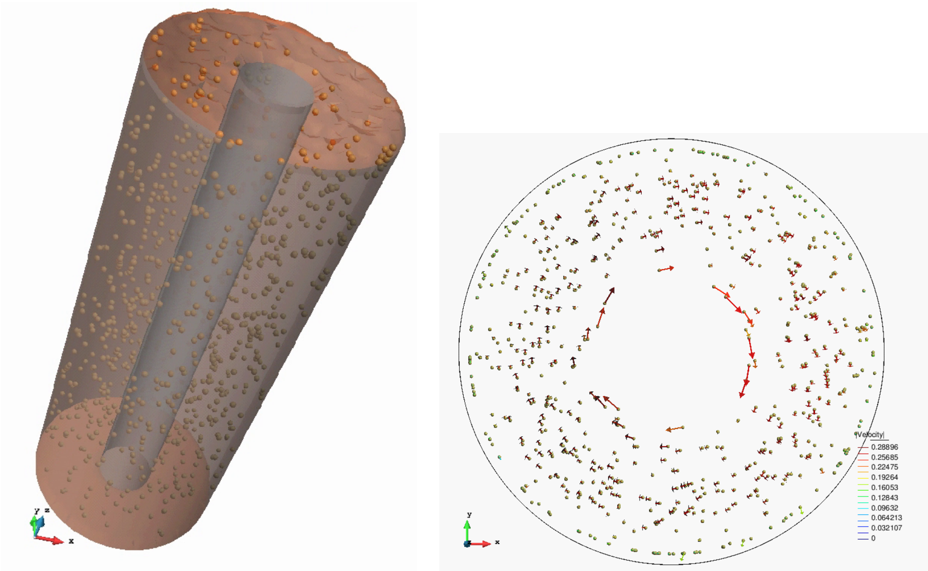

Fig. 6: Global view (left) and top view (rigth) of particles flowing at a rate of 1500 particles/(m^2s) within a vertical annulus. The centered drilling pipe rotates at 100 rpm

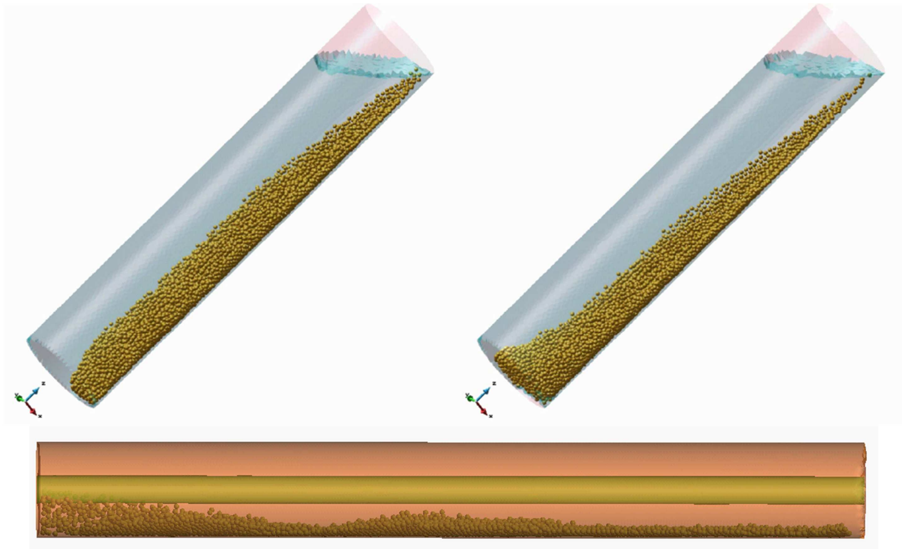

Fig. 7: Global view of an inclined (above) and horizontal (below) annulus carrying mud and cuttings at a rate of 1500 particles/(m^2s). The horizontal annulus includes a centered non-rotating drilling pipe

3.3 Cutting transport through more complex sections of the wellbore

The formulation presented has been tested with more complex geometries, like a section of the wellbore with a tool joint (Figure 9a) and a curved wellbore with a rotating drill string (100 r_{mp}) (Figure 9b). The fluid properties are the same as in Section 7.1. All the computations for these problems were carried out with PFEM.

In some of these problems beds can be formed. In such conditions, the drag forces are no longer accurate, since they are based on the assumption that the particles are disperse. This method should therefore used carefully, as no estimations of the error has been obtained in dense packing conditions. However, the examples shown prove the stability of the method in those situations.

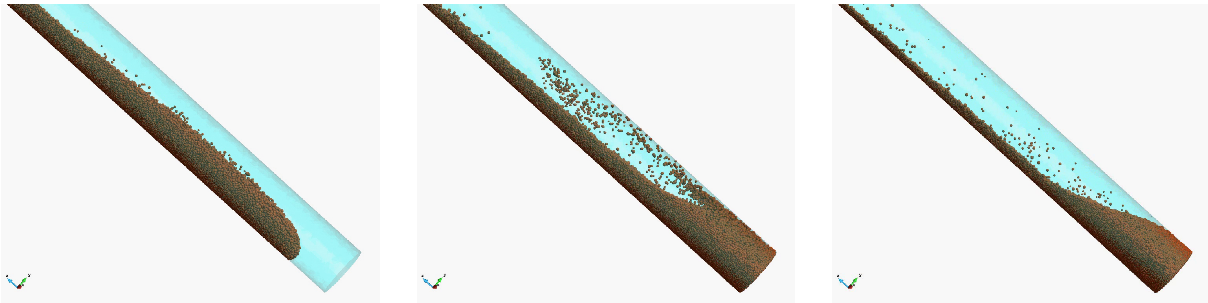

Fig. 8: Simulation of the accumulation of particles as they fall towards the bottom of a tube filled with mud

(a) (b)

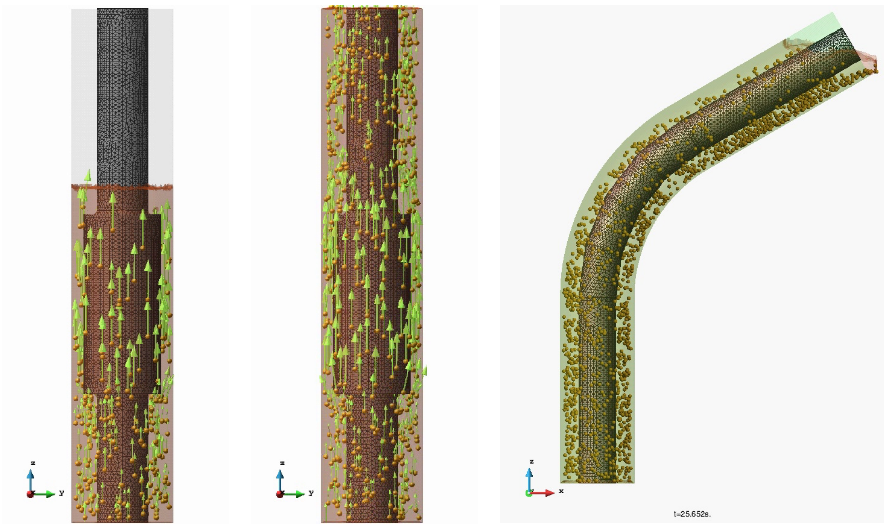

Fig. 9: Simulation of drill cuttings transported in straight and curved wellbores by mud as a result of a drilling operation. Arrows denote the velocity vector of each particle

4 CONCLUSIONS

A FEM-DEM technique has been presented to solve the transport of particles in non-Newtonian fluids which can be applied to wellbores full of circulating fluid, typical of the drilling industry. We have proposed a procedure for computing the drag force on the particles for non-Newtonian fluids using predictions of the terminal velocity available from the existing literature. The procedure has been extended to non-spherical particles, treating them as spheres in terms of contact forces but correcting the drag force according to the shape of the particles.

The usefulness of the proposed numerical method for studying the motion of the drill cuttings in vertical wellbores has been validated and the applicability and stability to other non-vertical and more complex configurations have been pointed out.

All of the developments done in terms of coupling between the non-Newtonian fluid and the DEM can be applied both to a Lagrangian PFEM approach for the fluid or to an Eulerian one. The coupling procedure is actually not dependent on the method used to solve the equations for the fluid. Therefore, it can be applied to other popular CFD methods, such as the Finite Volume Method (FVM) [40], the Lattice-Bolzmann Method (LBM) [41] or the Smoothed Particle Hydrodynamics (SPH) method [42]. This technique can also be combined with the erosion estimation methods published previously by the authors [11, 13].

Acknowledgements

This work was carried out with financial support by Weatherford. This research was also partially supported by project SAFECON of the European Research Council.

REFERENCES

1. Bourgoyne AT, Millheim KK, Chenevert ME, Young FS (1991) Applied Drilling Engineering. Society of Petroleum Engineers. Richardson, TX
2. Sifferman TR, Myers GM, Haden EL, Wahl HA (1974) Drill-Cutting Transport in Full-Scale Vertical Annuli. Journal of Petroleum Technology
3. Oñate E (1998) Derivation of stabilized equations for advective-diffusive transport and fluid flow problems. Comput. Meth. Appl. Mech. Engng. 151:233–267
4. Oñate E, Celigueta MA, Latorre S, Casas G, Rossi R, Rojek J (2014) Lagrangian analysis of multiscale particulate flows with the particle finite element method. Computational Particle Mechanics 1:85–102
5. Zohdi T (2007) An introduction to modelling and simulation of particulate flows. SIAM, Computational Science and Engineering
6. Cremonesi M, Frangi A, Perego U (2011) A Lagrangian finite element approach for the simulation of water-waves induced by landslides. Computers & Structures 89:1086–1093
7. Franci A, Oñate E, Carbonell JM (2015) On the effect of the bulk tangent matrix in partitioned solution schemes for nearly incompressible fluids. Accepted for publication in Int. J. Numer. Meth. Engng. DOI:10.1002/nme.4839
8. Idelsohn SR, Oñate E, Del Pin F (2004) The particle finite element method: a powerful tool to solve incompressible flows with free-surfaces and breaking waves. Int. J. Numer. Meth. Engng, 61(7):964–989
9. Idelsohn SR, Mier-Torrecilla M, Oñate E (2009) Multi-fluid flows with the Particle Finite Element Method. Comput Methods Appl Mech Engrg. 198:2750–2767
10. Oñate E, Idelsohn SR, Del Pin F, Aubry R (2004c) The particle finite element method. An overview. Int. J. Comput. Methods 1(2):267–307
11. Oñate E, Celigueta MA, Idelsohn SR (2006a) Modeling bed erosion in free surface flows by the Particle Finite Element Method, Acta Geotechnia 1(4):237–252
12. Oñate E, García J, Idelsohn SR, Del Pin F (2006c) FIC formulations for finite element analysis of incompressible flows. Eulerian, ALE and Lagrangian approaches. Comput. Meth. Appl. Mech. Engng. 195(23-24):3001–3037
13. Oñate E, Idelsohn SR, Celigueta MA, Rossi R (2008) Advances in the particle finite element method for the analysis of fluid-multibody interaction and bed erosion in free surface flows. Comput. Meth. Appl. Mech. Engng. 197(19-20):1777–1800
14. Oñate E (2009), Structural analysis with the finite element method. Volume 1. Basis and Solids. CIMNE-Springer
15. Oñate E, Celigueta MA, Idelsohn SR, Salazar F, Suárez B (2011) Possibilities of the particle finite element method for fluid-soil-structure interaction problems. Computational Mechanics, 48(3):307–318.
16. Oñate E, Franci A, Carbonell JM (2014) Lagrangian formulation for finite element analysis of quasi-incompressible fluids with reduced mass losses. Int. J. Num. Meth. in Fluids 74(10):699–731
17. Avci B, Wriggers P, (2012) A DEM-FEM coupling approach for the direct numerical simulation of 3D particulate flows. Journal of Applied Mechanics, 79(1), 7 pages
18. Cundall PA, Strack ODL (1979) A discrete numerical method for granular assemblies, Geotechnique 29:4765
19. Oñate E, Rojek J, (2004b) Combination of discrete element and finite element methods for dynamic analysis of geomechanics problems. Comput. Meth. Appl. Mech. Engrg. 193:3087–3128
20. Oñate E, Zárate F, Miquel J, Santasusana M, Celigueta MA, Arrufat F, Gandikota R, Ring KL (2015) A local constitutive model for the discrete element method. Application to geomaterials and concrete. Comp. Part. Mech 2(2):139–160
21. Clift R, Grace JR, Weber ME (1978) Bubbles, drops and particles. Academic Press, New York
22. Coussy O (2004) Poromechanics. Wiley
23. Zienkiewicz OC, Taylor RL, Zhu JZ (2005) The finite element method. The basis. 6th Ed., Elsevier
24. Zienkiewicz OC, Taylor RL, Nithiarasu P (2005) The finite element method for fluid dynamics. 6th Ed., Elsevier
25. Belytschko T, Liu WK, Moran B (2013) Non linear finite element for continua and structures. 2d Edition, Wiley
26. Donea J, Huerta A (2003) Finite element method for flow problems. J. Wiley
27. Jackson R (2000), The dynamics of fluidized particles. Cambridge Monographs on Mechanics, Cambridge Univ. Press
28. Best Practice Guidelines for Computational Fluid Dynamics of Dispersed Multiphase Flows. By SIAMUF, Swedish Industrial Association for Multiphase Flows, ERCOFTAC. 2008
29. Ansley RW, Smith TN (1967) Motion of spherical particles in a Bingham plastic. AIChE Journal 13(6):11931196

30. Brookes GF, Whitmore RL (1969) Drag forces in Bingham plastics. Rheologica Acta, 8(4):472–480
31. Kelessidis VC, Mpandelis G (2004) Measurements and prediction of terminal velocity of solid spheres falling through stagnant pseudoplastic liquids. Powder Technology 147
32. Chien SF (1994), Settling velocity of irregularly shaped particles, SPE Drill. Complet. 9 281
33. Shah SN, El Fadili Y, Chhabra RP (2007) New model for single spherical particle settling ve-locity in power law (visco-inelastic) fluids. International Journal of Multiphase Flow 33:51–66
34. Walker RE, Mayes TM (1975) Design of muds for carrying capacity. Journal of Petroleum Technology 27(7)
35. Walker RE (1976) Hydraulics limits are set by flow restrictions. Oil Gas Journal 86–90
36. Haider A, Levespiel O (1989) Drag coefficient and terminal velocity of spherical and nonspherical particles. Powder Technol. 58:6370
37. Oñate E (2004) Possibilities of finite calculus in computational mechanics. Int. J. Num. Meth. Engng. 60(1):255281
38. Kratos (2015) Open source software platform for multiphysics computations. CIMNE, Barcelona, www.cimne.com/kratos
39. GiD (2015). The personal pre/postprocessor. www.gidhome.com, CIMNE, Barcelona
40. Breuer M, Rodi W (1994). Large-eddy simulation of turbulent flow through a straight square duct and a 180^o bend. In Fluid Mechanics and its Applications, Vol. 26, Voke P.R., Kleiser L. and Hollet J.P. (Eds.). Direct and Large-Eddy Simulation I. Selected Papers from the First ERCOFTAC Workshop on Direct and Large-Eddy Simulation. Guildford, Surrey, UK, 2730 March 1994. Kluwer Academic Publishers, Dordrecht, pp. 273285
41. He X, Luo LS (1997) Lattice Boltzmann model for the incompressible NavierStokes equation. J. Stat. Phys., 88(34):927944
42. Monaghan JJ (1992) Smoothed particle hydrodynamics. Annu. Rev. Astron. Astrophys., 30:543–574